



HAL
open science

Long-term weathering rate of stained-glass windows using H and O isotopes

Loryelle Sessegolo, Aurélie Verney-Carron, Mandana Saheb, Laurent Remusat,
Adriana Gonzalez-Cano, Nicolas Nuns, Jean-Didier Mertz, Claudine Loisel,
Anne Chabas

► To cite this version:

Loryelle Sessegolo, Aurélie Verney-Carron, Mandana Saheb, Laurent Remusat, Adriana Gonzalez-Cano, et al.. Long-term weathering rate of stained-glass windows using H and O isotopes. *npj Materials Degradation*, 2018, 2, 10.1038/s41529-018-0038-1 . hal-03663303

HAL Id: hal-03663303

<https://hal.science/hal-03663303>

Submitted on 10 May 2022

HAL is a multi-disciplinary open access archive for the deposit and dissemination of scientific research documents, whether they are published or not. The documents may come from teaching and research institutions in France or abroad, or from public or private research centers.

L'archive ouverte pluridisciplinaire **HAL**, est destinée au dépôt et à la diffusion de documents scientifiques de niveau recherche, publiés ou non, émanant des établissements d'enseignement et de recherche français ou étrangers, des laboratoires publics ou privés.

ARTICLE OPEN

Long-term weathering rate of stained-glass windows using H and O isotopes

Loryelle Sessegolo¹, Aurélie Verney-Carron¹, Mandana Saheb¹, Laurent Remusat², Adriana Gonzalez-Cano², Nicolas Nuns³, Jean-Didier Mertz^{4,5}, Claudine Loisel^{4,5} and Anne Chabas¹

The understanding of glass alteration is a biogeochemical, industrial, societal (radioactive waste confinement), and cultural heritage issue. Studies have been mainly performed in aqueous conditions. However, glass reactivity under hydraulically unsaturated conditions may be more important than previously recognized. In this context, we evaluate here the role of the alteration layer formed on medieval stained-glass windows on the ongoing alteration in unsaturated conditions. H₂O adsorption isotherms were measured to study the relation between the vapor sorption and the relative humidity inside the alteration layer. From it, the average pore radius was calculated, yielding a water vapor diffusion coefficient of $7.8 \times 10^{-7} \text{ m}^2 \text{ s}^{-1}$ inside the pore network. Experiments using doped water vapor (D₂¹⁸O) confirm the vapor transport up to the alteration front via fractures and pore network. They also demonstrate that the alteration mainly progresses via an interdiffusion mechanism. The calculated interdiffusion coefficients at 20 °C are $3.6 \times 10^{-20} \text{ m}^2 \text{ s}^{-1}$ at 70% RH and $4.9 \times 10^{-20} \text{ m}^2 \text{ s}^{-1}$ at 90% RH, which is similar to the values measured on model stained-glass samples altered in short durations (1–4 years). Therefore, this study highlights that, given its morphology, the alteration layer is not protective against vapor transport and interdiffusion.

npj Materials Degradation (2018)2:17; doi:10.1038/s41529-018-0038-1

INTRODUCTION

Alteration of glass in aqueous media has been extensively studied in various contexts such as the geological storage of vitrified radioactive wastes, the contribution of basaltic glass dissolution to biogeochemical cycles, or the conservation of historical artifacts (e.g.,^{1–4} and references therein). Water is the main agent in glass degradation. This alteration induces the formation of an amorphous layer, mainly composed of Si and insoluble elements (e.g., Al, Zr), and of secondary phases. The formation of the amorphous layer (or gel layer) is still an open debate, as it can be explained by several mechanisms. In the first case, the gel layer is thought to be formed by hydration, interdiffusion, and hydrolysis/condensation reactions.^{5–7} Interdiffusion consists of an ion exchange between the glass-modifier cations (e.g., K⁺, Na⁺, and Ca²⁺) and hydrogenated species in solution (H⁺, H₂O, or H₃O⁺).^{6,7} It leads to the formation of a hydrated and dealkalinized layer that can be reorganized by local hydrolysis / condensation reactions.^{2,8,9} In the second case, an interfacial dissolution-precipitation process is proposed to explain the gel formation, notably on nuclear glass.^{10–12} More consensually, the secondary phases are formed by the precipitation of dissolved elements of the glass and/or elements of the environment. These mechanisms are similar in saturated (liquid water) and unsaturated media (water vapor), but their relative contribution is different. In the unsaturated medium, hydration and interdiffusion are considered to be major glass-alteration mechanisms.^{13–15}

Many studies have focused on the formation of the glass-alteration layer and its protective or passivating (hampering

further alteration) character, in particular, for nuclear glasses, since highly radioactive wastes are vitrified and intended to be buried in geological storage.^{15–17} Some of these works have highlighted a progressive pore closure and a change in the pore solution that decreases species diffusion within the alteration layer, and thus the alteration rate.^{8,18–26} This pore clogging is explained by the reorganization of the altered layer by hydrolysis and condensation of silicon.⁸ These results are deduced from the experiments of tracer circulation (dye or ²⁹Si) using time-of-flight/secondary-ion mass spectroscopy (ToF-SIMS)^{18,26} or from the measurement of the specific surface areas by small-angle X-ray scattering (SAXS)^{18,21} and by gas adsorption.¹⁸ Monte Carlo simulations are in agreement with the experimental results.^{20–22,26}

However, these experiments are mainly performed in a continuous aqueous medium. Recent studies carried out on nuclear glass in the presence of water vapor have highlighted the significant impact of vapor on glass alteration with substantial hydration depth and secondary phases precipitation.^{13,15,27–29} Nevertheless, it seems that there is no study assessing the role of the altered layer under these conditions. This question has also to be addressed in the case of stained-glass windows that are submitted to alternating saturated and unsaturated conditions for several centuries. The medieval Si–K–Ca glasses generally present high degradation states and thick altered layers.^{30–32} Their alteration layers are often very heterogeneous (in composition and structure^{31,33,34}) and fractured due to the wetting/drying cycles conditions.^{33,35,36} The crack network includes cracks parallel to the surface that are generally filled with secondary phases

¹LISA, UMR CNRS 7583, Université Paris-Est Créteil et Université Paris Diderot, Institut Pierre-Simon Laplace, 61, avenue du Général de Gaulle, 94010 Créteil Cedex, France; ²IMPMC, UMR CNRS 7590, UPMC, IRD, MNHN, CP52 57, rue Cuvier, Sorbonne Universités, 75231 Paris Cedex 05, France; ³Université Lille, CNRS, INRA, Centrale Lille, ENSCL, Université Artois, FR 2638 - IMEC - Institut Michel-Eugène Chevreul, 59000 Lille, France; ⁴CRC, Sorbonne Universités, USR 3224 CNRS, MNHN, Ministère de la Culture et de la Communication, CP21 Paris, France and ⁵LRMH, USR 3224, 29 rue de Paris, 77420 Champs-sur-Marne, France
Correspondence: Loryelle Sessegolo (loryelle.sessegolo@lisa.u-pec.fr)

Received: 24 January 2018 Revised: 16 April 2018 Accepted: 18 April 2018

Published online: 05 June 2018

(sulfates or carbonates) and unfilled perpendicular ones, so that water circulation can still occur within the altered layer up to the pristine glass interface.³⁵ Moreover, the exfoliation or detachment of altered glass scales can expose new surfaces to the atmosphere.³⁵ In this way, in contrast to the nuclear glasses, the influence of the pore closure over time on the alteration rate drop is expected to be low. Thus, the aim of the study is to trace water vapor circulation (using doped water in D₂¹⁸O) within the alteration layer of ancient stained-glass windows (already altered during 650 years) in order to assess its role and to investigate the progress of alteration to measure the long-term kinetics in unsaturated conditions.

RESULTS AND DISCUSSION

Two types of medieval stained-glass windows (14th century) named OU2 and EV1 were studied. These samples are not pristine: OU2 displays an alteration layer in the form of pits whose radius ranges between 50 and 200 μm. EV1 presents a continuous layer on its entire surface, of about 100 μm thick (see Supplementary material S1).

Before exposing these medieval glasses to doped water vapor at different relative humidity values (RH), the first step was to assess the relationship between the adsorbed water vapor content and the RH. For that, gravimetric measurements were carried out on the OU2 sample (which does not contain hygroscopic secondary phases) to obtain a moisture sorption isotherm at 25 °C, corresponding to the H₂O adsorption inside the pore network of the alteration layer (Fig. 1). The isotherm presents a strong hysteresis between the adsorption and desorption curves, generally associated with mesoporous material (pore diameter between 2 and 50 nm, from the IUPAC nomenclature³⁷). This hysteresis corresponds to a delay in vaporization, highlighting water condensation into the liquid state within the pore network at high RH. In order to build the isotherm curve, it was necessary that the weight gain reaches a stability (of the adsorption) for each RH value. The time to reach this equilibrium between the alteration layer and the fixed atmosphere depends on the surface available for adsorption and on RH. The lower the RH, the faster

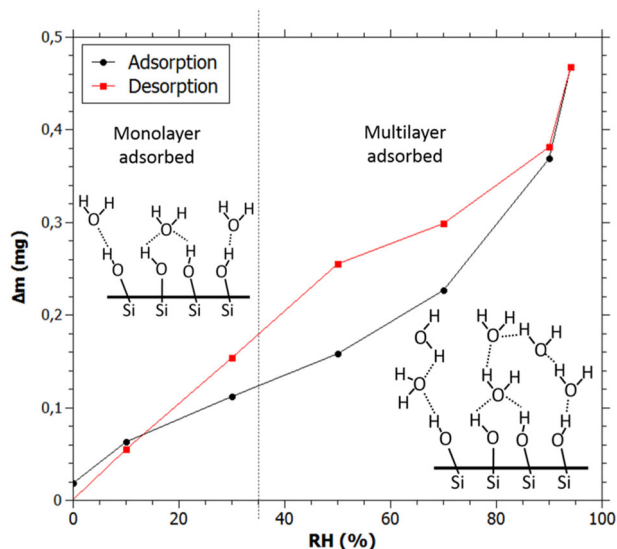


Fig. 1 Isotherm of H₂O adsorption/desorption determined by gravimetric measurements on one OU2 sample. Below 35% RH, the silica surface contains only the silanols/hydroxyls and the monolayer of water molecules adsorbed. Above 35% RH, the thickness of adsorbed water multilayers increases,³⁹ and the condensation occurs in the pore network at a RH value depending on the pore size

the equilibrium time (see Supplementary material S2). From there, at RH values of <35%, it is considered that only one monolayer of water molecules is adsorbed on the material, and at higher RH values, the number of layers of water molecules increases with RH³⁸ (Fig. 1). A second series of gravimetric measurements of H₂O adsorption was carried out to specifically study the range between 5 and 35% RH. Using the Brunauer, Emmett, and Teller (BET) theory³⁹ (Supplementary material Eq. S3-A to E and Fig. S3-A), it was possible to roughly calculate the specific surface area of the altered layer corresponding to the open porosity accessible by water vapor of 100 ± 40 m² g⁻¹, by assuming an average density of the alteration layer of 2.2 ± 0.5 (see ref. ⁴⁰) and an average alteration pit thickness of 100 ± 30 μm. Cailleateau et al.¹⁸ have found a specific surface of 84 ± 4 m² g⁻¹ after 39 days of leaching in aqueous media (63 ± 3 m² g⁻¹ after 125 days) associated with the total porosity (open and closed) by using small-angle X-ray scattering (SAXS), which is relatively close to the result of this present study.

By assuming that the altered layer contains micropores and mesopores, similar to what has been documented from previous studies on nuclear glasses,^{8,18,25} and from the shape of the isotherm, it is expected that at high RH, the water vapor condenses inside the pore network (according to the Kelvin's law, supplementary material Eq. S3-I and Fig. S3-B). Therefore, the weight gain at the highest RH value corresponds to the weight of liquid water in the pore volume, which then can be used to calculate an average pore radius of 2.0 ± 0.2 nm and an open porosity of 21% (Supplementary material Eq. S3-F). This pore size is in agreement with other recent studies concerning the alteration of nuclear glasses in aqueous media (between 1 and 40 nm for nuclear glass, as a function of glass composition^{8,18,25,40}) and less than 10 nm for ancient potash-lime silica glasses buried for several centuries.⁴¹

The Knudsen factor (K_n ; supplementary material Eq. S3-G) can be calculated from the knowledge of the previously estimated pore radius. K_n corresponds to the ratio of the mean free path for gas over the pore diameter size range (Supplementary material Eq. S3-G and S3-H). This factor can be used to distinguish between molecular diffusion (intramolecular collisions and Brownian motion), Knudsen diffusion (D_K ; Eq. 1) (describing molecule/pore wall collisions), and an intermediate transitional regime.⁴² If K_n is greater than 1, diffusion of vapor is mainly due to molecule/wall interactions and therefore is in the Knudsen diffusion regime.⁴³ For water vapor circulation inside the pores whose average radius is 2 nm, $K_n \gg 1$. The calculated Knudsen diffusion coefficient^{42,44,45} of the water vapor inside the altered layer is equal to $7.8 \times 10^{-7} \text{ m}^2 \text{ s}^{-1}$ (Eq. 1). From Fick's law (Eq. 2) and assuming an alteration layer thickness e of 230 μm (the maximum value for OU2 pits radius⁴⁴), the water vapor reaches the alteration front in 53 ms. This diffusion rate indicates that water vapor circulation is slowed (by 2 orders of magnitude) by the presence of the pore network, since the water vapor diffusion in the air is $2.82 \times 10^{-5} \text{ m}^2 \text{ s}^{-1}$ (25 °C).⁴⁶

$$D_K = \frac{2R_p}{3} \sqrt{\frac{8RT}{\pi M_i}} \quad (1)$$

With D_K , the Knudsen diffusion (in m² s⁻¹), R_p , the pore radius (in m), T , the temperature (in K), R , the ideal gas constant (in J mol⁻¹ K⁻¹), and M_i , the molar mass of the gas species (in kg mol⁻¹).

$$e = 2 \sqrt{\frac{D t}{\pi}} \quad (2)$$

With e , the alteration layer thickness (in m), D , the diffusion coefficient (in m² s⁻¹), and t , the time (in s).

The vapor circulation from the external surface to the alteration front is confirmed by the isotopic tracing experiment (using D₂¹⁸O), and the corresponding mapping of D and ¹⁸O distribution are carried out by NanoSIMS. All the enrichment values are

Table 1. ^{18}O and D average enrichment factor (f) of OU2 and EV1 alteration layers after the exposure to the doped vapor (measured by NanoSIMS)

OU2			
Time	RH (%)	$f(^{18}\text{O})$	$f(\text{D})$
1 day—S1	90	–	6.1 ± 0.0 ($n = 1$)
1 day—S2	90	–	5.3 ± 0.0 ($n = 1$)
2 months—S1	90	2.2 ± 0.2 ($n = 3$)	13.5 ± 3.9 ($n = 5$)
2 months—S2	90	1.9 ± 0.2 ($n = 3$)	12.8 ± 4.8 ($n = 12$)
2 months	40	1.6 ± 0.0 ($n = 1$)	7.9 ± 0.0 ($n = 1$)
2 months	25	1.4 ± 0.1 ($n = 2$)	–
2.75 months	70	1.7 ± 0.2 ($n = 7$)	–
14 months	90	2.5 ± 0.5 ($n = 7$)	25.7 ± 4.7 ($n = 6$)
EV1			
1 day	90	1.5 ± 0.1 ($n = 3$)	–
2 months	90	2.3 ± 0.5 ($n = 2$)	–
2 months	25	1.4 ± 0.2 ($n = 3$)	–
14 months	90	2.8 ± 0.3 ($n = 3$)	–

Average values are calculated from “ n ” different analyzed zones (whose surface area is $20 \times 20 \mu\text{m}^2$) carried out from the surface to the pristine glass interface on one sample. S1 and S2 correspond to the two series of analyses performed on the same sample at 1 year of interval

expressed in enrichment factors ($f(\text{D})$ and $f(^{18}\text{O})$), with respect to natural abundances for more convenience:

$$f(\text{D}) = \frac{(\text{D}/\text{H})_{\text{sample}}}{(\text{D}/\text{H})_{\text{natural}}} \quad (3)$$

$$f(^{18}\text{O}) = \frac{(^{18}\text{O}/^{16}\text{O})_{\text{sample}}}{(^{18}\text{O}/^{16}\text{O})_{\text{natural}}} \quad (4)$$

EV1 and OU2 samples were exposed for 1 day at 90% RH and 20 °C under doped water vapor (D_2^{18}O). The isotopic distribution inside the alteration layer reveals the presence and the homogeneity of the isotopic enrichments, from the external surface to the pristine glass interface (Table 1). No diffusion gradient is observable. Nevertheless, even if the water vapor reaches the alteration front rapidly (in agreement with the vapor diffusion coefficient determined previously), no sign of an alteration progress, which would correspond to the local enrichments at the altered/pristine glass interface, was detected in this short exposure time. The medieval glasses that were exposed for 2 months at 25, 40, and 90% RH (20 °C) under the doped vapor also presented homogeneous isotopic enrichments of D and ^{18}O throughout the altered layers. The enrichments values are higher than for the 1 day of exposure and linearly increases as a function of RH between 25 and 90% RH, whatever the isotope D or ^{18}O (Fig. 2a; Table 1). Furthermore, the isotopic enrichments of ^{18}O are similar for OU2 and EV1 samples at 25 and 90% RH, despite the different morphologies of their alteration layer (Fig. 2a; Table 1). The same observations can be done for samples exposed for 14 months (Fig. 2b; Table 1). The evolution of the isotopic enrichments as a function of time is not linear and tends toward a plateau or at least a decrease in the enrichment sorption, and seems to stabilize for ^{18}O from 2 months of exposure (Fig. 2b).

These enrichments measured using NanoSIMS inside the alteration layers result from a sequence of different processes: (1) a sorption process where water vapor molecules are physically adsorbed at the surface of the altered layer due to Van Der Waals forces, (2) an isotopic exchange of D and ^{18}O from doped vapor

with H and ^{16}O , respectively, that are contained in the alteration layer, (3) a desorption process at the end of the experiment when samples are stored in a desiccator (at 14 %RH), and (4) a new isotopic exchange of D and ^{18}O of the sample with H and ^{16}O contained in the vapor of the desiccator.

Processes (1) and (3) are described by the sorption isotherm curve (Fig. 1). Process (2) occurs at the surface of the pore network. Indeed, this latter is mainly composed of silanols Si-OH (as Al and Fe contents are low, see the glass compositions in the Supplementary material S1). A monolayer of adsorbed water is strongly bonded to the hydroxyl group (Si-OH---H₂O) and is always present, even at very low RH or under vacuum.³⁸ The higher the RH, the higher is the accumulation of water molecules layers adsorbed above this monolayer,³⁹ which increases the species available for isotopic exchange. Therefore, the exchange of H and O isotopes between Si- ^{16}OH and the monolayer of the adsorbed D_2^{18}O can explain the influence of RH on the level of the enrichment (and the linear increase observed on Fig. 1a). In order to study these isotopic exchange processes between vapor and silica surface (processes (2) and (4) in the sequence), three OU2 samples have been exposed for 2 weeks to D_2^{18}O vapor at 90% RH (20 °C) and then were submitted to three different post-treatments. The average isotopic enrichments inside the entire alteration layer have been measured using ToF-SIMS. The first sample, setting as a reference, was stored in the desiccator after isotopic exposure and displayed D and ^{18}O enrichments (Table 2). The second sample was heated after the doped vapor exposure for 2 h at 190 °C. Compared to the reference sample, the heated sample showed a depletion of D enrichment by 20% and only 2.5% of ^{18}O enrichment (Table 2). Considering that the heating of the sample at this temperature leads to desorption of all the free and adsorbed water on the silica surface,³⁸ even the monolayer strongly bonded to the hydroxyls (Si-OH---H₂O), which leaves only silanols Si-OH, this means that 20% of the D enrichment corresponds to the monolayer of water molecules absorbed at the pore surface and 80% takes part in the silanol/hydroxyl groups. This confirms that H atoms of the hydroxyls were exchanged with D atoms of the water vapor. Concerning oxygen, ^{18}O enrichment has decreased by 2.5% after heating, which indicates that very few ^{18}O was contained in the adsorbed monolayer of water molecules and the majority of ^{18}O had been exchanged within the hydroxyl groups. Therefore, there is a difference in the isotopic exchange affinity between both the isotopes. The third sample was exposed, after doped vapor exposure, to 100% RH for 2 weeks with H_2O water vapor (at 20 °C) to see if the isotopic exchanges are reversible or not. The depletion is of 13 and 10% for D and ^{18}O enrichments, respectively (Table 2). This indicates that a new exposure at very high RH and the certainly at liquid-state water (pore condensation at 100% RH) induced a new isotopic exchange at a relatively similar rate for both isotopes in these conditions. However, the depletion is weak, which shows that the exchange rate is slow. This is confirmed at lower RH during storage (in a desiccator at 14% RH, desorption process (4) in the sequence) by two analyses of the sample OU2 altered for 2 months at 90% RH at 1 year of interval (S1 and S2 series, Table 1). The ^{18}O enrichment of S2 has decreased by 11% and the D enrichment by 14%, compared to S1 (Table 1). For OU2 sample altered for 1 day at 90% RH, the D enrichment is lower by 13% after 1 year (Table 1). Thus, the losses after 1 year of storage are similar for D and ^{18}O , and this inverse isotopic exchange is much slower than at very high RH (100% RH). This can be explained by the fact that at 14% RH, very few water molecules are adsorbed and are available for an isotopic exchange, whereas at 100% RH, liquid water condensation in the pores is expected (Fig. S3-B in the supplementary material), accelerating the exchange processes.

The progress of alteration during the experiment is initiated by the high content of adsorbed water in the pore network at high

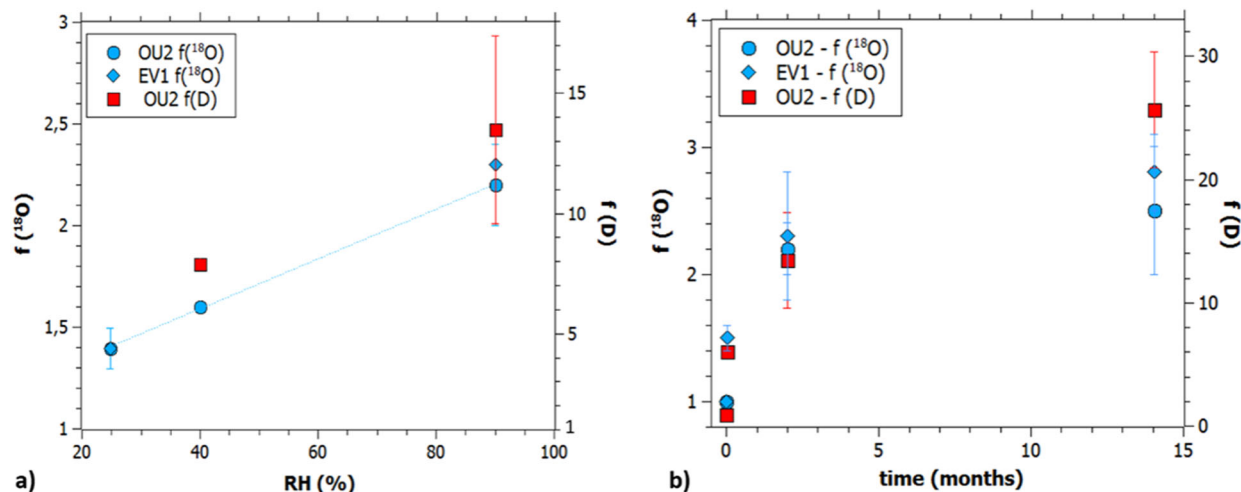


Fig. 2 Evolution of ^{18}O and D enrichment factors **a** as a function of RH (in %) for 2 months of exposure and **b** as a function of time at 90% RH (0, 0.03, 2, and 14 months). Values presented in **(a, b)** come from S1 series. Errors are given at the 1 σ confidence interval; if not visible, they are smaller than the symbols

Table 2. Average values of the ^{18}O and D enrichment factors (f) after different post-treatments for OU2 exposed to D_2^{18}O vapor for 2 weeks at 90% RH (measured by ToF-SIMS)

	$f(^{18}\text{O})$	$f(\text{D})$
D_2^{18}O	2.82 ± 0.02	3.62 ± 0.12
$\text{D}_2^{18}\text{O} + \text{Heating}$	2.75 ± 0.02	2.91 ± 0.23
$\text{D}_2^{18}\text{O} + \text{H}_2\text{O}$	2.54 ± 0.02	3.16 ± 0.12

The first sample (D_2^{18}O) was just stored in desiccator after experiment. The second ($\text{D}_2^{18}\text{O} + \text{Heating}$) was heated at 190 °C. The third one ($\text{D}_2^{18}\text{O} + \text{H}_2\text{O}$) was subjected to H_2O vapor at 100% RH for 2 weeks. One analysis was performed for each sample in the cross-section, on a $100 \times 100 \mu\text{m}^2$ area, covering the entire alteration layer

RH, and by eventual capillary condensation expected to occur at lower RH than 100% in the pore network (from about 60% RH for 2 nm pores, according to the Kelvin's law, supplementary material Eq. S3-l). This is confirmed by the observation of interfaces showing strong local D enrichments for several samples at high RH: 2 months at 90% RH, 2.75 months at 70% RH, and 14 months at 90% RH. The interfacial enrichments are only observed for D (Fig. 3c, f) and not for ^{18}O (Fig. 3a, d). The local D enrichments are located at all the interfaces with pristine glass, at the glass-alteration front (Fig. 3f), as well as at the interface of 'islets' of low-altered glass within the altered layer of OU2 (Fig. 3c). These isolated islets, surrounded by the alteration layer, are caused by the previous tree-like progress of the alteration. NanoSIMS mappings indicate that the small islets are entirely enriched in D, 'disappearing' under the enrichment, whereas the largest ones keep a core not enriched in D (Fig. 3c). These observations highlight a progress of alteration by an interdiffusion mechanism involving only or mainly the hydrogen isotopes, since local enrichment in ^{18}O is not observable. The absence of ^{18}O enriched rims reveals that, at this stage, there is no interdiffusion of D_2^{18}O water molecules, and no hydrolysis/condensation (or precipitation) reactions is occurring at the interface with the pristine glass. Moreover, some very local spots are extremely enriched with a D enrichment factor up to 150 (e.g., red zones on Fig. 3c, f). The observation of the same areas using SEM (in Back-Scattered Electron mode, BSE) after the experiment indicates that these extremely enriched zones correspond to the modified glass areas (Supplementary material S4). Indeed, visually, the morphology

evolves from that of the pristine glass, fairly clear and uniform, to a progressively darker zone (on SEM images), similar to hydrated or altered glass (Supplementary material S4). These darker areas have low intensity, which indicates the replacement of glass elements by lighter elements (from water) and possibly the development of porosity, therefore the evolution of the hydrated glass. However, these spots do not display ^{18}O enrichment, highlighting that in these zones there is no hydrolysis/condensation reactions yet. Indeed, if local hydrolysis/condensation reactions or interfacial dissolution/precipitation have occurred, ^{18}O would be included in the newly formed siloxane bonds, as it is observed and proposed by Geisler et al.¹⁰ In this study, the preliminary step in the formation of the alteration layer (that occurred during the experiment only in unsaturated conditions) seems to be only interdiffusion.

In order to determine the thickness of D^+ interdiffusion inside the pristine glass, image processing was carried out to superimpose the SEM images and the associated NanoSIMS mapping (Fig. 4d-h). The enriched layer thicknesses are variable and sometimes correspond to an accumulation of D at the interface, but also to the interdiffusion in the pristine glass. The superimposition allowed both contributions to be differentiated. The average interdiffusion thickness is about 0.6 μm for the sample exposed 2.75 months at 70% RH (Fig. 4d-f) and about 1.5 μm for the sample exposed 14 months at 90% RH (Fig. 4g, h). By knowing this deuterium diffusion thickness (e) and the alteration time (t), and by applying the Fick's law (Eq. 2), the interdiffusion coefficient corresponding to the ion exchange can be deduced: $3.6 \times 10^{-20} \text{ m}^2 \text{ s}^{-1}$ for the sample weathered at 70% RH and $4.9 \times 10^{-20} \text{ m}^2 \text{ s}^{-1}$ for the sample at 90% RH.

The values of the interdiffusion coefficients are much higher in the aqueous medium or the buried medium (in soil). For buried archeological Si-K-Ca medieval glasses (9 and 13th), Sterpenich et al.⁴⁷ have found a diffusion coefficient of around $1 \times 10^{-17} \text{ m}^2 \text{ s}^{-1}$. Few studies have measured interdiffusion coefficients of glass in atmospheric medium. Cummings et al.⁴⁸ have performed experiments on modern soda-lime glass samples at different temperatures (40, 70, and 90 °C) and RH from 10% to 95% RH. By converting their data (hydration rate in $\mu\text{m h}^{0.5}$) in interdiffusion coefficient and roughly fitting the curve of D vs. RH by an exponential law, we could deduce the interdiffusion coefficients of $1.1 \times 10^{-21} \text{ m}^2 \text{ s}^{-1}$ at 70% RH and $1.7 \times 10^{-21} \text{ m}^2 \text{ s}^{-1}$ at 90% RH (at 40 °C). Then the activation energy was calculated at 70 and 90% RH, and the interdiffusion coefficients at 20 °C were extrapolated using the Arrhenius' law on the Cummings' data. These coefficients are

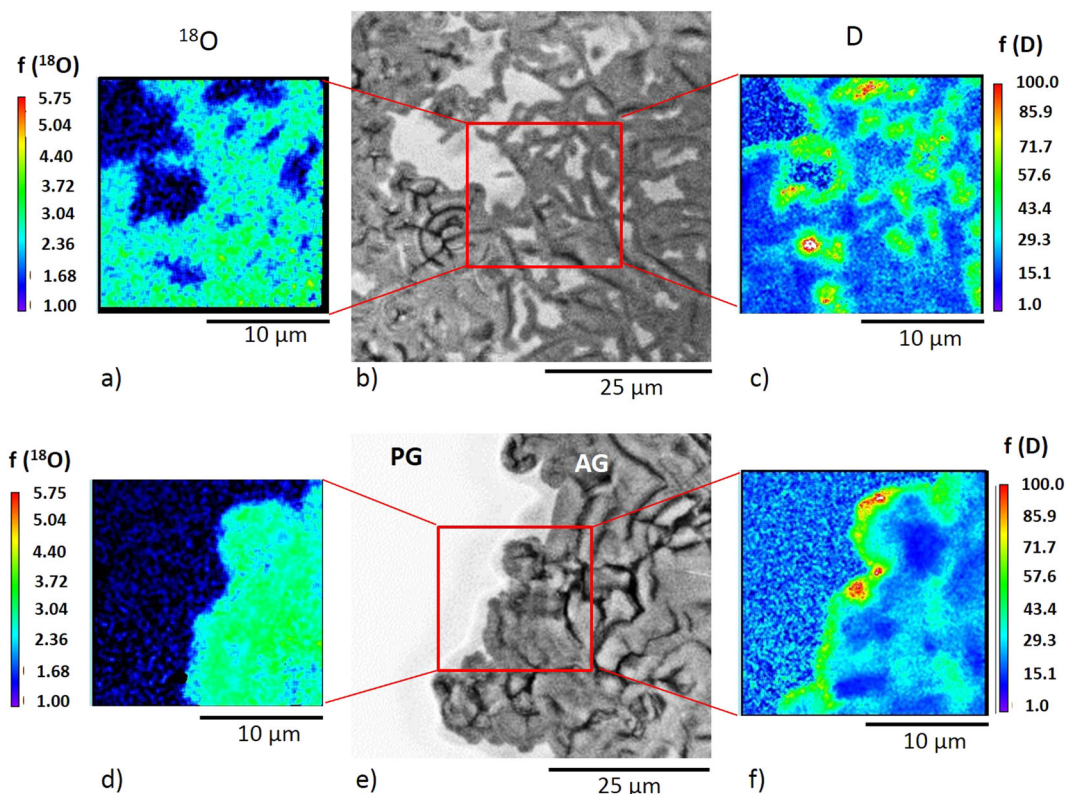


Fig. 3 $^{18}\text{O}/^{16}\text{O}$ and D/H mapping on two zones of OU2 sample at 90% RH for 14 months. The scale is expressed in enrichment factor with respect to the natural abundances. **b**, **e** SEM-BSE images of the analyzed zones: **b** is in the middle of the alteration layer, which contains isolated low-altered glass islets, and **e** is the pristine glass interface. **a**, **d** are $^{18}\text{O}/^{16}\text{O}$ mapping associated to each zone, and **c**, **f** are D/H mapping associated to the same zones. PG, pristine glass; AG, altered glass

$1.8 \times 10^{-22} \text{ m}^2 \text{ s}^{-1}$ at 70% RH and $2.5 \times 10^{-22} \text{ m}^2 \text{ s}^{-1}$ at 90% RH. These values are lower than the values in this study, as the glass composition is richer in silica and more durable, but the increase factor of the coefficients between 70 and 90% RH is 1.4, which is identical to the increase factor of this study between the same RH values. Furthermore, Gentaz⁴⁹ have exposed model glasses (whose composition is close to the old stained-glass windows of this study) in real atmosphere and in sheltered conditions in Paris. The alteration layer after 36 months is $1.2 \mu\text{m}$, which corresponds to a diffusion coefficient of $1.2 \times 10^{-20} \text{ m}^2 \text{ s}^{-1}$ (using the Fick's law, Eq. (2)) for an average RH of 76% and an average temperature of 12°C . This short-term diffusion coefficient on model glasses is therefore slightly lower than the long-term coefficients found in this study due to the lower temperature, but they are in the same order of magnitude, demonstrating that the interdiffusion coefficients are similar at short and long-alteration term.

A last point is to determine whether D enrichment is really due to the interdiffusion during the experiment (between D^+ and $\text{K}^+/\text{Ca}^{2+}$) and not due to isotopic exchange (between D^+ and H^+) in the hydrated layer already formed before the experiment (during the 650 years of atmospheric conditions). As previously mentioned, the morphology of some highly D enriched areas (red spots, Fig. 3f and S4 in the supplementary material) highlights the evolution of the pristine glass into a more porous and hydrated phase, which seems to indicate the progress of the modifier exchange with D^+ . Furthermore, EDS analyses were performed on an isolated islet inside the altered layer in order to measure the composition differences between the pristine glass; the islet core and 2 zones at the alteration front of the islet: one in the middle of the D enriched area and the other one at the same distance of the alteration front, but in the non-D enriched area (Points 1, 2, and 3 on Fig. 4c). These analyses allowed verification that the core of this

large glass islet (Point 3 on Fig. 4c) has a composition very close to that of the pristine glass (PG, Table 3). Furthermore, the D enriched zone shows a depletion in glass-modifier cations (Point 1 on Fig. 4c; Table 3) higher than the non-enriched zone just close to it (Point 2 on Fig. 4c; Table 3). The contents in K_2O and CaO for point 1 are 5.4 and 7.9 wt.%, respectively, whereas for point 2, the K_2O and CaO contents are 8.6 and 10.2 wt.%, respectively. This is accompanied by a relative increase of the SiO_2 content that is almost 8 wt.% higher for the D enriched zone, compared to the non-D enriched zone. The depletion in the modifier cations (K^+ , Ca^{2+} , and Mg^{2+}) highlights that the interdiffusion process occurs between the deuterium and the modifiers cations, and not only by exchange between the deuterium and the hydrogen due to the hydration during the 650 years of the atmospheric exposure.

Finally, Verney-Carron et al.⁵⁰ have led the same experiment on EV1 sample with a light rain doped in D_2^{18}O . They have also found D enrichments located at the pristine glass interfaces and have calculated a deuterium diffusion coefficient of $2.8 \times 10^{-18} \text{ m}^2 \text{ s}^{-1}$ using the Fick's law (Eq. 2). Therefore, it is possible to combine both the studies to calculate the rain and the vapor contributions (with the interdiffusion coefficient values determined in this study at 70 and 90% RH). From the Fick's law and considering that it is raining 6% of the time in Paris (548 h year^{-1} in average between 1961 and 1990 at Paris Montsouris, Meteofrance data), the rain contribution to the alteration thickness after 650 years is $66 \mu\text{m}$ and the vapor contribution ranges between $31 \mu\text{m}$ (for 70% RH) and $35 \mu\text{m}$ (for 90% RH). The total altered-layer thickness for 650 years of alteration is about $100 \mu\text{m}$, in good agreement with real thicknesses observed in ancient samples (between 50 and $200 \mu\text{m}$).^{30,33,34} This also shows that the contribution of RH on the alteration thickness is significant and has to be considered.

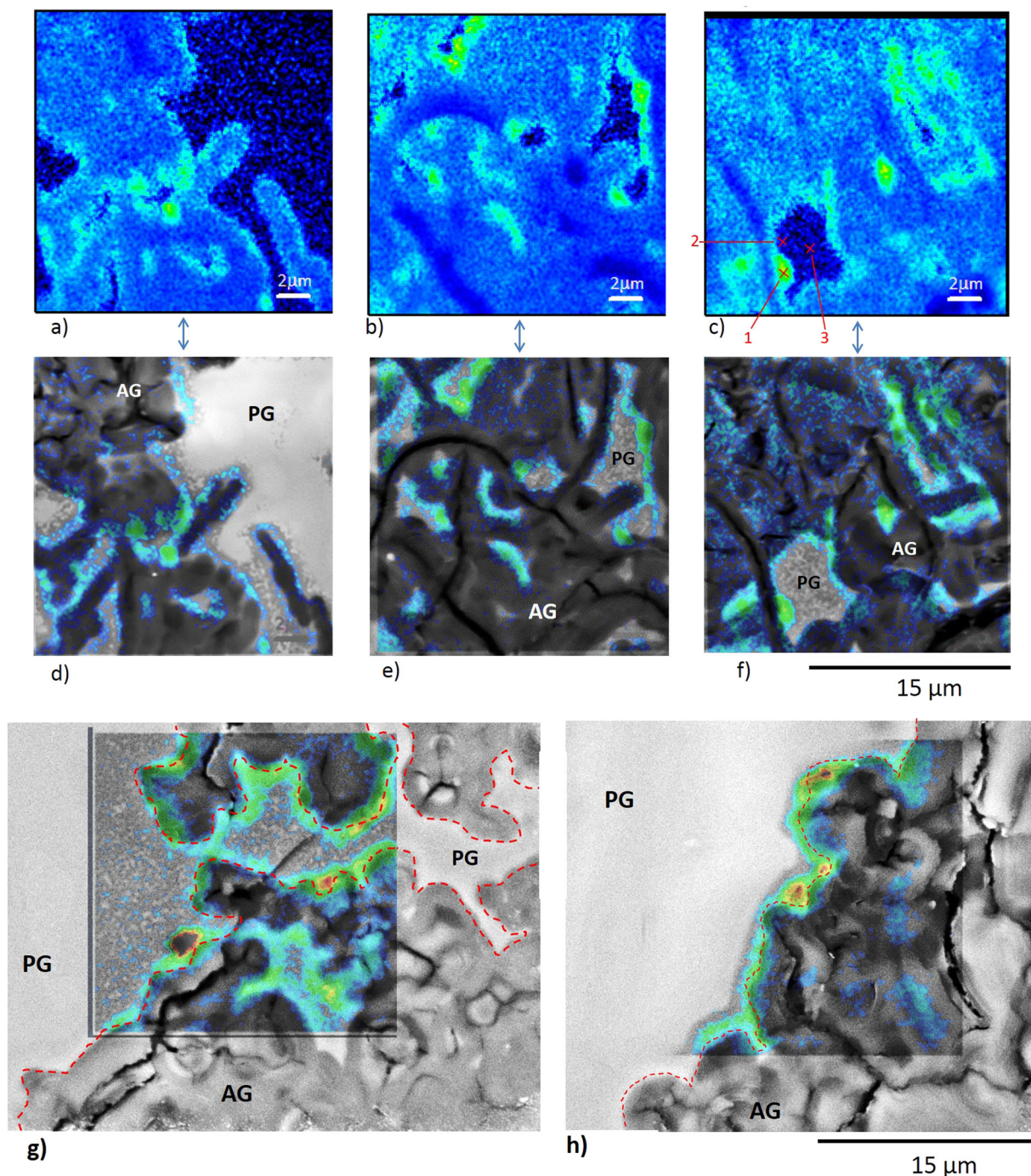


Fig. 4 **a–c** D/H NanoSIMS mappings of the OU2 sample exposed 2.75 months at 70% RH and **d–f** are the corresponding overlay by image processing on the SEM-BSE images. **a, d** are located at the pristine glass interface. **b, c, e, and f** are located in the middle of the alteration layer, with D penetration inside the isolated islets of low-altered glass. **g, h** are the overlays by image processing of the D/H mappings on the associated SEM-BSE images of two zones of the OU2 sample exposed for 14 months at 90% RH. In all these images, the green zones and rims correspond to the local highly D enriched areas with the D penetration inside the pristine glass. PG, pristine glass; AG, altered glass. It should be noted that the grayish edges in front of the enrichments in the pristine glass (images **d, h** especially) do not correspond to the hydrated zone, but to artifacts of the image processing. These edges are not present on the initial SEM images

In conclusion, this study yields insights into the progress of the alteration of medieval stained-glass windows in unsaturated media and demonstrates that it is mainly caused by an interdiffusion mechanism between H^+ (or D^+) and the glass modifiers. This long-term alteration rate is quantified and is expressed as an interdiffusion coefficient that is comparable to the short-term exposure values of the model samples. This can be

explained by an important fracture network from the external surface to the alteration front, creating undoubtedly the major vector of liquid water in the rain events, but also a vector for water vapor. In addition, this study can be used to assess some pore network characteristics of a stained-glass window sample. Even if these results are not representative of the broad morphologies panel of the altered layers, they highlight the importance of the

Table 3. Chemical composition measured by SEM-EDS

Zones	Na ₂ O	MgO	Al ₂ O ₃	SiO ₂	P ₂ O ₅	K ₂ O	CaO	MnO	Fe ₂ O ₃
PG	2.5	6.8	1.0	57.8	3.6	12.7	13.8	0.7	0.6
AG	0.3	1.7	1.9	82.5	2.2	3.6	6.0	0.6	1.3
1	0.9	3.6	1.5	76.6	2.5	5.4	7.9	0.6	1.0
2	1.4	4.8	1.5	68.8	3.3	8.6	10.2	0.6	0.9
3	2.0	6.7	1.2	61.8	3.4	11.2	12.5	0.6	0.6

PG, pristine glass, AG, altered glass. Points 1, 2, and 3 are associated with the three analyzed zones on the Fig. 4c. Point 1 is on the D-enriched zone, point 2 is close to point 1, but not D-enriched, and point 3 is located in the core of the low-altered glass islet

total characterization of the pore network, giving access to the different diffusion processes associated. The case of atmospheric conditions is particularly complicated because it combines two water phases (liquid and gas) in the same system. Indeed, the liquid water does not depend solely on a rain episode soaking up the entire weathering layer, but also on the pore size and its distribution, which will create, depending on the relative humidity, the condensation of water. Therefore, the water diffusion mechanisms in the altered layer (pores and cracks) are mixed in unsaturated medium and have to be studied and combined in further works to properly define the actual diffusion rates of hydrogenated species up to the pristine glass.

MATERIALS AND METHODS

Glass samples

The studied stained-glass windows samples come from the Saint-Ouen Abbey Church in Rouen (OU2) and the Notre-Dame Cathedral of Evreux (EV1), both in the North of France. Fragments of these glasses were set aside during a restoration of the monuments in the 1960–1970's. They date from the 14th century and have therefore been weathered for more than 600 years by the atmospheric conditions. They have consequently developed very thick alteration layers. The composition of the pristine glass and the alteration layer was previously determined.³³ For OU2, on the external face, the altered layer is discontinuous in thickness and consists of large pits (up to 1 mm across and 230 μm depth⁴⁹). In addition, some pits exhibit a tree-like structure evolution, insulating some “islets” of the pristine glass in the altered layer. Furthermore, the crack network is highly developed and displays thin and dense cracks that are not filled with secondary phases. For EV1, the altered layer of the external face is continuous all along the surface. The crack network is composed of very large fractures filled with secondary phases (syngenite CaK₂(SO₄)₂·H₂O). A more complete description of the morphology and composition of pristine and altered glass is given in the Supplementary material S1.

Exposure experiments

The objective of these experiments was to study the role of the altered layer on the further alteration of the ancient stained-glass windows. Thus, pieces of OU2 and EV1 were exposed to a controlled atmosphere in climatic chambers. Three sealed boxes were partly filled with super-saturated saline solutions: K₂SO₄ for 90% RH, K₂CO₃ for 40% RH, and CH₃COOK for 25% RH, at 20 °C.⁵¹ The relative humidity values achieved, measured using a Vaisala data logger, are 91.1 ± 3.0% RH, 40.9 ± 2.0% RH, and 28.8 ± 2.0% RH. The boxes were placed in a temperature-controlled chamber at 20 °C (± 1 °C). OU2 and EV1 stained-glass samples were exposed for different durations: 1 day at 90% RH, 2 months at 90, 40, 25% RH, 2.75 months at 70% RH, and 14 months at 90% RH. All samples were placed inside each box above, but not in contact with the saline solutions. In order to trace the water penetration and reactions sites in the altered layer, the water of the saline solutions was enriched in ¹⁸O and D. The water composition was 10% of H₂¹⁸O and 90% of D₂O (Eurisotop®). The ¹⁸O/¹⁶O ratio in solution was 0.110 and the D/H ratio was 8.9. The natural ratios from the SMOW (Standard Mean Ocean Water) are 2.05 × 10⁻³ and 1.15 × 10⁻⁴, respectively. Before and after analyses, the samples were stored in a desiccator (at 14% RH). Finally, some samples were altered in order to

clarify the isotopic adsorption process inside the altered layer. Three OU2 samples were exposed for 2 weeks at 90% RH in D₂¹⁸O. The first sample was placed in a desiccator before the embedding and the ToF-SIMS analyses. The second sample was heated at 190 °C in order to remove all the physically adsorbed water³⁸ for 2 h and directly embedded after the heating. The third sample was placed in a chamber at 100% RH in H₂O vapor for 2 weeks after the doped vapor exposure.

Analytical techniques

After exposure, the samples were embedded in resin (Korapox®), polished (from grade P800 of SiC abrasive paper to the ¼ μm diamond powder, using ethanol), and coated with gold to allow cross-section observations. Microphotographs were acquired using a tabletop LV-SEM TM3030 Hitachi, a low-vacuum SEM equipped with energy dispersive spectrometer Quantax 70 EDS Bruker. An accelerating voltage of 15 kV in charge-up reduction mode has been used. Compositions were determined with a Field emission SEM Jeol JSM-6301F fitted with an EDS Silicon Drift X-Max 80 mm² detector and Aztec Advanced-INCA350 analyzer, Oxford Instruments, at 20 kV. Samples were analyzed using a Cameca NanoSIMS (Secondary Ion Mass Spectrometry). This instrument provides ¹⁸O/¹⁶O and D/H mapping, but also provides the elemental mapping of Si, C, and S. A primary Cs⁺ beam (1.5 pA for ¹⁸O analyses and 40–50 pA for D analyses) was used to scan the sample surface over 20 × 20 μm² area (256 × 256 pixels, 1 ms/pixel) and the secondary ions of the elements were collected. One session was done to measure Si, C, S, ¹⁶O, and ¹⁸O and a second one to measure H⁺ and D⁺. The analyzed chamber vacuum was at about 7 × 10⁻¹⁰ Torr. An electron-flooding gun was used to compensate for charge defects. Before each analysis, a presputtering on 25 × 25 μm² area (high primary current for 20 min for ¹⁸O analyses, 10 min for D analyses) was applied to remove the gold coating and surface contamination, and to reach a steady state sputtering.⁵² The data were expressed in the enrichment factor *f*(D) and *f*(¹⁸O) (see Eq. (3) and (4)). Uncertainties (at 1σ) were calculated using the propagation law combining the counting statistic (between 40 and 60 scans), and the standard deviation of the values obtained for different mappings on the same sample. Data processing was performed using the Limage software (L. Nittler, Carnegie Institution in Washington DC), and the enrichment values were obtained by selecting only the amorphous silica matrix of the altered layer. The areas of precipitated phases (mainly syngenite for EV1), the resin zones, the pristine glass, and the interfacial enrichments were all subtracted to obtain only the value of the amorphous silica phase.

ToF-SIMS analyses of D/H and ¹⁸O/¹⁶O were done with a ToF-SIMS⁵ from IONTOF. Primary ion beam was generated from a bismuth source in burst mode (25 kV) to avoid hydrogen and ¹⁶O detector saturation. Cs⁺ (140 nA, 2 kV) were used for sputtering. Before each analysis, a presputtering was performed over an area of 300 × 300 μm² for 5 min to remove the palladium coating. Analyses (100 × 100 μm²) were done with burst mode (6 pulses) for the oxygen isotopes analyses, and in burst-alignment mode for the hydrogen isotopes. All the analyses were carried out with a Cs⁺ sputtering (for 1 s) between each scan of analysis, and a low energy (20 eV) electron-flooding gun was used to compensate positive charge due to the primary ion beam. The number of scans for one measurement varied between 515 and 620, and for each scan, the number of pixels was 256 × 256. Data were also expressed in enrichment factor. Uncertainties were calculated from errors on the Poisson correction applied on measurements (for dead time effects of the registration system).⁵³

Gravimetric measurements of H₂O adsorption at 25 °C were carried out using a device IGA-sorp (Hidden Isochema). Two faces of a blank were polished to remove the altered layers. The polishing was done from grade P1000 to grade ¼ μm to remove any scratches that could enhance the surface adsorption of the glass. Between 0 and 93% RH, the blank gains 1% of its mass. This reference corresponds to the support bracket plus the sample (blank) whose two faces were polished. The specific surface of the blank was calculated using the BET theory and is negligible (0.2 m² g⁻¹). The adsorption tests have only been carried out on an OU2 sample that contains few crystallized salts. Indeed, EV1 is constituted of many syngenites in the crack network, which has an important hygroscopic effect. Three tests were carried out: two to confirm the isotherm and one to assess the range of RH values, in which BET theory (monolayer adsorption) is linear. The adsorption durations for each RH step were long enough to reach the weight gain equilibrium, before moving to the next RH step (see Supplementary material S2). The uncertainty threshold of the mass variation was 5%. Uncertainties on the calculated specific surface area are relatively high due to the important standard deviation of the

craters thickness and of the density that increases the uncertainty on the alteration layer mass. It is important to note that the calculated specific surface area corresponds to the BET application of monomolecular adsorption layer on a partially dehydrated initial pore surface because the OU2 sample has been pre-treated by storage and heat at 60 °C for 1 week. However, these conditions are closer to adsorption in real atmospheric conditions, and avoid the increase of cracks, the destabilization of the alteration layer, and in particular, of the pore network, due to high temperature.

Finally, the overlay of the NanoSIMS mapping and SEM images was accomplished by image processing software, in which the layers were merged in the subtraction mode, and to specific color desaturations to bring out only interfacial enrichments and not the silicate matrix (of the PG or AG). The resulting maps were fitted to SEM images using precise landmarks (such as low-altered glass islets or highly enriched spots) that coincide between the mappings and the images.

Data availability

The data that support the findings of this study are available from the corresponding author upon reasonable request.

ACKNOWLEDGEMENTS

The authors would like to thank the French National Research Agency (ANR) for their financial support (ANR GLAM). The NanoSIMS Facility at MNHN was funded by CNRS, Région Île de France, Ministère délégué à l'Enseignement supérieur et à la Recherche and MNHN. The authors are grateful to Patrick Ausset for the SEM-EDS analyses. This work was supported by the French National Research Agency (ANR).

AUTHOR CONTRIBUTIONS

A.V.C. and A.C. supervised the study. L.S. was responsible for experimental analysis and wrote the paper. M.S. was involved in data interpretation. L.R. and A.G.C. performed the NanoSIMS analyses. N.N. performed the ToF-SIMS analyses. J.D.M. performed the adsorption tests by gravimetric measurements. C.L. provided the stained-glass windows samples and advices on data interpretation. All the authors helped in paper editing.

ADDITIONAL INFORMATION

Supplementary information accompanies the paper on the *npj Materials Degradation* website (<https://doi.org/10.1038/s41529-018-0038-1>).

Competing interests: The authors declare no competing interests.

Publisher's note: Springer Nature remains neutral with regard to jurisdictional claims in published maps and institutional affiliations.

REFERENCES

- Gin, S. et al. An international initiative on long-term behavior of high-level nuclear waste glass. *Mater. Today* **16**, 243–248 (2013).
- Verney-Carron, A. et al. Understanding the mechanisms of Si–K–Ca glass alteration using silicon isotopes. *Geochim. Cosmochim. Acta* **203**, 404–421 (2017).
- Verney-Carron, A., Gin, S. & Libourel, G. Archaeological analogs and the future of nuclear waste glass. *J. Nucl. Mater.* **406**, 365–370 (2010).
- Dessert, C., Dupré, B., Gaillardet, J., François, L. M. & Allègre, C. J. Basalt weathering laws and the impact of basalt weathering on the global carbon cycle. *Chem. Geol.* **202**, 257–273 (2003).
- Lanford, W. A. et al. Hydration of soda-lime glass. *J. Non-Cryst. Solids* **33**, 249–266 (1979).
- Doremus, R. H. Interdiffusion of hydrogen and alkali ions in a glass surface. *J. Non-Cryst. Solids* **19**, 137–144 (1975).
- Wassick, T. A., Doremus, R. H., Lanford, W. A. & Burman, C. Hydration of soda-lime silicate glass, effect of alumina. *J. Non-Cryst. Solids* **54**, 139–151 (1983).
- Gin, S. et al. Origin and consequences of silicate glass passivation by surface layers. *Nat. Commun.* **6**, 6360 (2015).
- Bouakkaz, R., Abdelouas, A., Mendili, Y. E., Grambow, B. & Gin, S. SON68 glass alteration under Si-rich solutions at low temperature (35–90 °C): kinetics, secondary phases and isotopic exchange studies. *RSC Adv.* **6**, 72616–72633 (2016).
- Geisler, T. et al. Aqueous corrosion of borosilicate glass under acidic conditions: a new corrosion mechanism. *J. Non-Cryst. Solids* **356**, 1458–1465 (2010).

- Geisler, T. et al. The mechanism of borosilicate glass corrosion revisited. *Geochim. Cosmochim. Acta* **158**, 112–129 (2015).
- Hellmann, R. et al. Nanometre-scale evidence for interfacial dissolution–reprecipitation control of silicate glass corrosion. *Nat. Mater.* **14**, 307–311 (2015).
- Abrajano, T. A., Bates, J. K. & Mazer, J. J. Aqueous corrosion of natural and nuclear waste glasses II. Mechanisms of vapor hydration of nuclear waste glasses. *J. Non-Cryst. Solids* **108**, 269–288 (1989).
- Chaou, A. A., Abdelouas, A., Mendili, Y. E., Bouakkaz, R. & Martin, C. The French SON68 glass vapor hydration under different atmospheres. *Proc. Mater. Sci.* **7**, 179–185 (2014).
- Chaou, A. A. et al. Vapor hydration of a simulated borosilicate nuclear waste glass in unsaturated conditions at 50 °C and 90 °C. *RSC Adv.* **5**, 64538–64549 (2015).
- Ojovan, M. I. & Lee, W. E. Immobilisation of radioactive wastes in glass. in *An Introduction to Nuclear Waste Immobilisation* 213–249 (Kidlington, Oxford, U.K: Elsevier, 2005).
- Pierce, E. M., Rodriguez, E. A., Calligan, L. J., Shaw, W. J. & Pete McGrail, B. An experimental study of the dissolution rates of simulated aluminoborosilicate waste glasses as a function of pH and temperature under dilute conditions. *Appl. Geochem.* **23**, 2559–2573 (2008).
- Cailleteau, C. et al. Insight into silicate-glass corrosion mechanisms. *Nat. Mater.* **7**, 978–983 (2008).
- Frugier, P. et al. SON68 nuclear glass dissolution kinetics: current state of knowledge and basis of the new GRAAL model. *J. Nucl. Mater.* **380**, 8–21 (2008).
- Ledieu, A., Devreux, F., Barboux, P. & Minet, Y. Contribution of Monte Carlo modeling to understanding the alteration of nuclear glasses by water. *Nucl. Sci. Eng.* **153**, 285–300 (2006).
- Arab, M. et al. Aqueous alteration of five-oxide silicate glasses: experimental approach and Monte Carlo modeling. *J. Non-Cryst. Solids* **354**, 155–161 (2008).
- Jégou, C., Gin, S. & Larché, F. Alteration kinetics of a simplified nuclear glass in an aqueous medium: effects of solution chemistry and of protective gel properties on diminishing the alteration rate. *J. Nucl. Mater.* **280**, 216–229 (2000).
- Rebiscoul, D., Frugier, P., Gin, S. & Ayral, A. Protective properties and dissolution ability of the gel formed during nuclear glass alteration. *J. Nucl. Mater.* **342**, 26–34 (2005).
- Rebiscoul, D. et al. Morphological evolution of alteration layers formed during nuclear glass alteration: new evidence of a gel as a diffusive barrier. *J. Nucl. Mater.* **326**, 9–18 (2004).
- Rebiscoul, D. et al. Water dynamics in nanoporous alteration layer coming from glass alteration: an experimental approach. *J. Phys. Chem. C* **119**, 15982–15993 (2015).
- Jollivet, P. et al. Investigation of gel porosity clogging during glass leaching. *J. Non-Cryst. Solids* **354**, 4952–4958 (2008).
- Bates, J. K., Seitz, M. G. & Steindler, M. J. The relevance of vapor phase hydration aging to nuclear waste isolation. *Nucl. Chem. Waste Manage.* **5**, 63–73 (1984).
- Gong, W. L. et al. Analytical electron microscopy study of surface layers formed on the French SON68 nuclear waste glass during vapor hydration at 200 °C. *J. Nucl. Mater.* **254**, 249–265 (1998).
- Neeway, J. et al. Vapor hydration of SON68 glass from 90 °C to 200 °C: A kinetic study and corrosion products investigation. *J. Non-Cryst. Solids* **358**, 2894–2905 (2012).
- Sterpenich, J. & Libourel, G. Using stained glass windows to understand the durability of toxic waste matrices. *Chem. Geol.* **174**, 181–193 (2001).
- Carmona, N., Villegas, M. A. & Navarro, J. M. F. Characterisation of an intermediate decay phenomenon of historical glasses. *J. Mater. Sci.* **41**, 2339–2346 (2006).
- Salviulo, G., Silvestri, A., Molin, G. & Bertoncello, R. An archaeometric study of the bulk and surface weathering characteristics of Early Medieval (5th–7th century) glass from the Po valley, northern Italy. *J. Archaeol. Sci.* **31**, 295–306 (2004).
- Lombardo, T. et al. Long term assessment of atmospheric decay of stained glass windows. *Corros. Eng. Sci. Technol.* **45**, 420–424 (2010).
- Lombardo, T. et al. Characterisation of complex alteration layers in medieval glasses. *Corros. Sci.* **72**, 10–19 (2013).
- Gentaz, L. et al. Role of secondary phases in the scaling of stained glass windows exposed to rain. *Corros. Sci.* **109**, 206–216 (2016).
- Gentaz, L., Lombardo, T., Loisel, C., Chabas, A. & Vallotto, M. Early stage of weathering of medieval-like potash-lime model glass: evaluation of key factors. *Environ. Sci. Pollut. Res. Int.* **18**, 291–300 (2011).
- Rouquerol, J. et al. Recommendations for the characterization of porous solids (Technical Report). *Pure Appl. Chem.* **66**, 1739–1758 (2009).
- Zhuravlev, L. T. The surface chemistry of amorphous silica. Zhuravlev model. *Colloids Surf. Physicochem. Eng. Asp.* **173**, 1–38 (2000).
- Brunauer, S., Emmett, P. H. & Teller, E. Adsorption of gases in multimolecular layers. *J. Am. Chem. Soc.* **60**, 309–319 (1938).
- Collin, M. et al. Structure of international simple glass and properties of passivating layer formed in circumneutral pH conditions. *Npj Mater. Degrad.* **2**, 4 (2018).

41. Cooper, G. I. & Cox, G. A. A comparative study of the natural and experimental corrosion of poorly durable potash-lime-silica glasses. *MRS Online Proc. Libr. Arch.* **333**, 525 (1993).
42. Knudsen, M. Die Gesetze der Molekularströmung und der inneren Reibungsströmung der Gase durch Röhren. *Ann. Phys.* **333**, 75–130 (1909).
43. Chambre, P. A. & Schaaf, S. A. *Flow of Rarefied Gases*. (Princeton University Press, Princeton, 1961).
44. Kennard, E. H. *Kinetic Theory of Gases: With an Introduction to Statistical Mechanics*. (McGraw-Hill Book Company, New York, 1938).
45. Present, R. D. *Kinetic Theory of Gases*. (McGraw-Hill Book Company, New York, 1958).
46. Cussler, E. L. *Diffusion: Mass Transfer in Fluid Systems*. (Cambridge University Press, Cambridge, 1997).
47. Sterpenich, J. & Libourel, G. Water diffusion in silicate glasses under natural weathering conditions: evidence from buried medieval stained glasses. *J. Non-Cryst. Solids* **352**, 5446–5451 (2006).
48. Cummings, K., Lanford, W. A. & Feldmann, M. Weathering of glass in moist and polluted air. *Nucl. Instrum. Methods Phys. Res. Sect. B* **136–138**, 858–862 (1998).
49. Gentaz, L. Simulation et modélisation de l'altération des verres de composition médiévale dans l'atmosphère urbaine. PhD thesis of Paris-Est Creteil University, 264 pp. (2011).
50. Verney-Carron, A., Saheb, M., Loisel, C., Duhamel, R. & Remusat, L. Use of hydrogen isotopes to understand stained glass weathering. *Procedia Earth Planet. Sci.* **13**, 64–67 (2015).
51. Greenspan, L. Humidity fixed points of binary saturated aqueous solutions. *J. Res. Nat. Bur. Stand. Sect. Phys. Chem.* **81A**, 89 (1977).
52. Thomen, A., Robert, F. & Remusat, L. Determination of the nitrogen abundance in organic materials by NanoSIMS quantitative imaging. *J. Anal. At. Spectrom.* **29**, 512–519 (2014).
53. Stephan, T., Zehnpfenning, J. & Benninghoven, A. Correction of dead time effects in time-of-flight mass spectrometry. *J. Vac. Sci. Technol. Vac. Surf. Films* **12**, 405–410 (1994).



Open Access This article is licensed under a Creative Commons Attribution 4.0 International License, which permits use, sharing, adaptation, distribution and reproduction in any medium or format, as long as you give appropriate credit to the original author(s) and the source, provide a link to the Creative Commons license, and indicate if changes were made. The images or other third party material in this article are included in the article's Creative Commons license, unless indicated otherwise in a credit line to the material. If material is not included in the article's Creative Commons license and your intended use is not permitted by statutory regulation or exceeds the permitted use, you will need to obtain permission directly from the copyright holder. To view a copy of this license, visit <http://creativecommons.org/licenses/by/4.0/>.

© The Author(s) 2018